Raman scattering tensors in tetragonal WO_3

M. Govender[1, 2], A. G. J. Machatine[1], H. W. Kunert[1], P. Niyongabo[1], and B. W. Mwakikunga[2]

[1]Department of Physics, University of Pretoria, Pretoria 0002, South Africa
[2]DST/CSIR National Centre for Nano-Structured Materials, P. O. Box 395, Pretoria 0001, South Africa

E-mail: MGovender2@csir.co.za and Augusto.Machatine@up.ac.za

Abstract. The matrix elements of the Raman scattering tensors are constructed from the Clebsch-Gordan coefficients (CGC's). Using group theoretical Birman's method, we calculate the CGC's of the tetragonal phase tungsten trioxide α-WO_3 with the space group D_{4h}^7. These obtained scattering tensors are used in the interpretation of the Raman spectra.

1. Introduction

Experimental data relies on proper interpretation to understand what the results are trying to convey to us. In this study, α-WO_3, which is to be used as the active sensing material in gas sensors, are characterized with Raman spectroscopy [1]. In Raman spectroscopy, laser light is incident on the sample under investigation, and this interaction causes the creation or destruction of the Raman-active optical phonons (longitudinal optical (LO) and transverse optical (TO)) [2]. The energy difference between the incident light and scattered light is equivalent to the Raman-shift. The observed Raman peaks are assigned to certain lattice vibrations which are contained in the lattice mode representations. The symmetry of the Raman-active modes are determined by the symmetrized square Kronecker Product (KP) of the vector representation [V⊗V] $_{(2)}$ of a space group in a crystal [3]. The excitations in the crystal are classified according to irreducible representations (irreps) of a space group.

2. Theoretical background

The Raman polarizability is the quantum analogue of the second-order tensor and describes the change in the electric polarizability produced by an excitation of the crystal [4]. The Raman scattering tensor $P_{\alpha\beta}\left(\bar{R}\right)$ is related to the crystal polarizability tensor through the relation [4, 5]

$$P_{\alpha\beta}\left(\bar{R}\right)= P_{\alpha\beta}^{(0)}\left(\bar{R}^0\right)+\sum_{j\sigma}P_{\alpha\beta}^{(1)}\left(\bar{R}^0;j\sigma\right)Q_\upsilon^j +\sum_{jj'}\sum_{\sigma\sigma'}P_{\alpha\beta}^{(2)}\left(\bar{R}^0;j\sigma;j'\sigma'\right)Q_\upsilon^jQ_{\upsilon'}^{j'} +..., \quad (1)$$

where the symbols in Equation (1) have been defined in [5]. Polarizability tensor is an expansion of a power series of normal coordinates Q_υ^j.

Scattering tensors relate the Cartesian components of the scattered radiation field to those of the incident field [5]. The elements of the first-order Raman scattering tensor are precisely linear combinations of certain Clebsch-Gordan coefficients (CGC's) [6]. CGC's are matrix elements of the unitary matrix U that brings the KP into a full reduced form. In order to calculate the CGC's, we need the matrix representations of the groups and their selections rules. The Cracknell, Davies, Miller and Love (CDML) tables [7] contain the characters and matrix generators of the 230 space groups at high symmetry point's throughout the respective Brillouin zones. The tables also contain the symmetrized squares, anti-symmetrized squares and cubes for the 230 space group irreps.

The α-WO$_3$ falls in the $P4/nmm\left(D_{4h}^7\right)$ space group, and Figure 1 shows the Brillouin zone of the simple tetragonal lattice. The point of highest symmetry is represented by the point Γ in Figure 1. It is at this point that Raman spectroscopy is concerned with, resulting from the phonon wavelength λ (same order of magnitude as the excitation laser wavelength ~5000 Å) typically being much greater than the lattice constant a (~5 Å) of the crystal structure [2]. It is also important to note that the interaction of the other points within the Brillouin zone (eg. points Δ, X) may contribute to the Raman (second-order scattering) intensity at the Γ point, and hence a direct contribution to the Raman peaks.
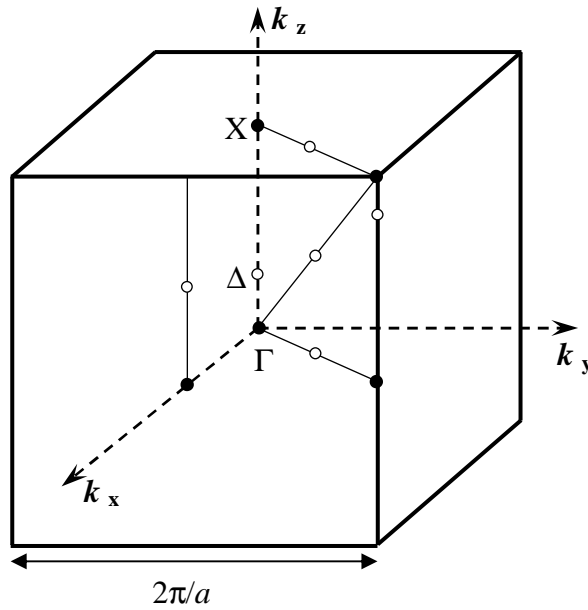
Figure 1. The Brillouin zone for simple cubic tetragonal lattice [7].

In this work, the matrix elements of the unitary matrix U, whose coefficients are certain linear combinations of CGC's, will be determined and used to construct one-phonon first-order Raman scattering tensors. These tensors will be validated against literature.

3. Clebsch-Gordan coefficients and scattering tensors

The determined vector representation (V-rep) of D_{4h}^7 using CDML tables [7] is given by

$$V = B_{1u} \oplus E_u = \Gamma_{3-} \oplus \Gamma_{5-}. \tag{2}$$

The ordinary KP is given by the following equation

$$\begin{aligned}
[V \otimes V] &= [\Gamma_{3-} \otimes \Gamma_{3-}] \oplus [\Gamma_{3-} \otimes \Gamma_{5-}] \oplus [\Gamma_{5-} \otimes \Gamma_{3-}] \oplus [\Gamma_{5-} \otimes \Gamma_{5-}] \\
&= \quad \Gamma_{1+} \quad\quad \oplus \quad\quad \Gamma_{5+} \quad\quad \oplus \quad\quad \Gamma_{5+} \quad\quad \oplus \Gamma_{1+} \oplus \Gamma_{2+} \oplus \Gamma_{4+}.
\end{aligned} \tag{3}$$

The Raman-active modes are contained in the symmetrized square KP and is given by

$$\begin{aligned}
[V \otimes V]_{(2)} &= [\Gamma_{3-} \otimes \Gamma_{3-}]_{(2)} \oplus [\Gamma_{5-} \otimes \Gamma_{5-}]_{(2)} \\
&= \quad \Gamma_{1+} \quad\quad \oplus \quad\quad \Gamma_{1+} \oplus \Gamma_{2+} \oplus \Gamma_{4+}.
\end{aligned} \tag{4}$$

The number of Raman-active modes observed in the spectrum is contained in the total number of lattice mode representations. In other words, the number of Raman-active modes shown in Equation (4) does not necessarily have a one-to-one correspondence to the number of experimentally observed Raman peaks.

The calculated CGC's are presented in Table 1. The CGC's for the symmetrized square of the V-rep is contained in the first three columns and the anti-symmetrized V-rep is contained in the last two columns.

Table 1. Clebsch-Gordan Coefficeints for D_{4h}^7.

| $[\Gamma_{3-} \otimes \Gamma_{3-}]_{(2)} \oplus [\Gamma_{5-} \otimes \Gamma_{5-}]_{(2)} =$ | Γ_{1+} $\oplus$ | Γ_{2+} $\oplus$ | Γ_{4+} | | |
$[\Gamma_{3-} \otimes \Gamma_{5-}] = [\Gamma_{5-} \otimes \Gamma_{3-}] =$				Γ_{5+}	
xx	$1/\sqrt{2}$	$-1/\sqrt{2}$	0	0	0
xy	0	0	$1/\sqrt{2}$	0	0
xz	0	0	0	$1/\sqrt{2}$	0
yx	0	0	$1/\sqrt{2}$	0	0
yy	$1/\sqrt{2}$	$1/\sqrt{2}$	0	0	0
yz	0	0	0	0	$1/\sqrt{2}$
zx	0	0	0	$1/\sqrt{2}$	0
zy	0	0	0	0	$1/\sqrt{2}$
zz	1	0	0	0	0

For completeness, the linear combination of the CGC's gives the first-order scattering tensor matrices given as

$$A_{1g} : \Gamma_{1+} = \frac{1}{\sqrt{2}} \begin{pmatrix} 1 & 0 & 0 \\ 0 & 1 & 0 \\ 0 & 0 & \sqrt{2} \end{pmatrix}, \quad A_{2g} : \Gamma_{2+} = -\frac{1}{\sqrt{2}} \begin{pmatrix} 1 & 0 & 0 \\ 0 & -1 & 0 \\ 0 & 0 & 0 \end{pmatrix}, \quad B_{2g} : \Gamma_{4+} = \frac{1}{\sqrt{2}} \begin{pmatrix} 0 & 1 & 0 \\ 1 & 0 & 0 \\ 0 & 0 & 0 \end{pmatrix},$$

$$E_g : \Gamma_{5+}^{(1)} = \frac{1}{\sqrt{2}} \begin{pmatrix} 0 & 0 & 1 \\ 0 & 0 & 0 \\ 1 & 0 & 0 \end{pmatrix}, \text{ and } E_g : \Gamma_{5+}^{(2)} = \frac{1}{\sqrt{2}} \begin{pmatrix} 0 & 0 & 0 \\ 0 & 0 & 1 \\ 0 & 1 & 0 \end{pmatrix}. \tag{5}$$

These CGC's can be used to construct various scattering tensors such as Brillouin scattering tensors and scattering tensors for morphic effects [6]. Therefore, the determination of CGC's is of great interest to experimentalists due to its versatility amongst the scattering techniques by manipulating the combinations of the same set of the CGC's for the space group relevant to the technique involved.

4. Experimental results

To confirm that the prepared tungsten oxide in question falls under the relevant space group, x-ray diffraction was carried out on the sample under investigation. For more information about the synthesis and type of sample, refer to Govender et al [8]. Carrying out an analysis on the corresponding x-ray spectrum shown in Figure 2 (a), it was found to match well with tetragonal phase ($P4/nmm$) WO_3 under PDF reference number 01-085-0808. The broad peak present in this spectrum results from the SiO_2 ($P2$ space group) substrate [9]. The corresponding Raman spectrum presented in Figure 2 (b) can now be analysed.
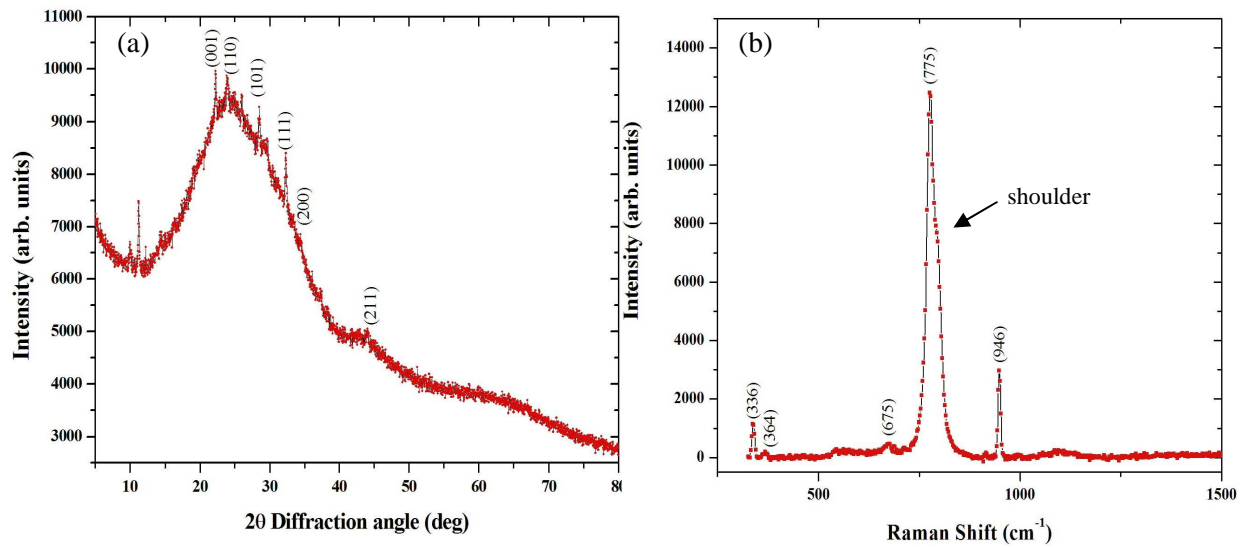
Figure 2. (a) The XRD spectrum of a WO_3 that shows characteristic peaks of a tetragonal phase and (b) the Raman spectrum of the tetragonal phase WO_3 thin film

According to literature [10], the two strong peaks at 775 cm^{-1} and 946 cm^{-1} in Figure 2 (b) does not result from tetragonal phase WO_3. These two peaks result from the combined contribution of both tetrahedral borate groups and WO_6 groups which most probably arise from the substrate. From this result, these peaks are not related to our scattering tensors. Looking closer at the 775 cm^{-1} peak, there is a shoulder at ~800 cm^{-1} which is expected for α-WO_3 [11], and this contributes to the overall intensity of that peak. The peak at 336 cm^{-1} is a blue-shifted peak from the literatures 326 cm^{-1}, and the 675 cm^{-1} is a red-shifted peak from the literatures 682 cm^{-1} [11]. It is evident that the shifts are approximately the same amount, and so it is probable that the shape and size of the material caused this shift since we are comparing the spectra of nanobelts to that of thin films [12]. The origins of the peak at 364 cm^{-1} is not known, and so other processes such as two-phonon processes, forbidden modes and morphic effects need to be considered [6].

The relative Raman intensities of the stretching modes is given by the ratio of the square of the scattering tensors for B_{2g} Γ_{4+} and A_{1g} Γ_{1+}, and the value comes out to be $1/3$. From this analysis, we speculate that the shoulder peak at 800 cm^{-1} is assigned to the A_{1g} Γ_{1+} mode and the peak at 336 cm^{-1} is assigned to B_{2g} Γ_{4+} mode. For proper and accurate assignments of the peaks and modes, polarization must be conducted [12].

5. Summary and discussion

In this work, we focused on the construction of first-order Raman scattering tensors for space group D_{4h}^7, using well known group theoretical methods. The ordinary KP gives $\Gamma_{1+} \oplus \Gamma_{2+} \oplus \Gamma_{4+} \oplus \Gamma_{5+}$ phonon modes. The Γ_{5+} comes from $[\Gamma_{3-} \otimes \Gamma_{5-}]$, and this mode is not contained in the symmetrized square of the V-rep. Therefore, the Γ_{5+} mode belongs to the anti-symmetrized part of the V-rep and contributes to the Raman spectra through some other mechanism. Following from relevant selection rules, CGC's can be obtained, and the appropriate combination of these coefficients gives information about a particular scattering process. To the authors' knowledge, this is the first time that the CGC's for the D_{4h}^7 group have been calculated, and was shown in Table 1. We obtained an estimation of the relative intensities of the Raman peaks using the scattering tensors to identify the stretching modes. Accurate assignments will be carried out when Raman polarization studies and lattice dynamics for this phase of WO_3 are obtained. Future work involves derivation of higher-order scattering tensors, Raman cross-sections, and relaxation times. The study carried out is the first step in the elucidation of a gas sensing mechanism when using α-WO_3. To experimentalists and device engineers, this information may assist in the design of such a specialized device.

References

[1] Boulova M, Gaskov A, and Lucazeau G, 2001, Tungsten oxide reactivity versus CH4, CO and NO molecules studied by Raman spectroscopy, *Sensors and Actuators B 81* pp. 99-106.
[2] Loudon R, 2001, The Raman effect in crystals, *Advances in Physics 50, No.7* pp. 813-864.
[3] Kunert H W, 2004, Scattering tensors for semiconductors of C_{6v}^4-P6$_3$ mc space group: GaN, ZnO, CdS, ZnS, and BeO, *Eur. Phys. J. Appl. Phys. 27* pp. 309-312.

[4] Cardona M, 1983, Light Scattering in Solids I Introductory Concepts, *Springer-Verlag Berlin Heidelberg New York*.

[5] Birman J L and Bereson R, 1974, Scattering and Clebsch-Gordan coefficients in crystals, *Phys. Rev. B 9, No. 10* pp. 4512-4517.

[6] Berenson R, 1981, Scattering Tensors and Clebsch-Gordan Coefficients in Crystals: Brillouin and Morphic Effects, *J. Phys. Chem. Solids 42*, pp. 391-404.

[7] Cracknell A P, Davies B L, Miller S C and Love W F, 1979, *Kronecker Product Tables* Ifl/Plenum, New York, Washington

[8] Govender M, Shikwambana L, Mwakikunga B W, Sideras-Haddad E, Erasmus R M, and Forbes A, 2011, Formation of tungsten oxide nanostructures by laser pyrolysis: stars, fibres and spheres, *Nanoscale Research Letters 6*, pp. 1-8.

[9] Boisen M B, Gibbs G V and Bukowinski M S T, 1994, *Phys. Chem. Minerals* 21 pp. 269-284.

[10] ElBatal F H, 2009, Gamma ray interaction with lithium borate glasses containing WO_3, *Indian Journal of Pure and Applied Physics 47* pp. 471-480.

[11] Wu W, Yu Q, Lian J, Bao J, Liu Z and Pei S-S, 2010, Tetragonal tungsten oxide nanobelts synthesized by chemical vapor deposition, *Journal of Crystal Growth 312* pp. 3147–3150.

[12] Livneh T, Lilach Y, Popov I, Kolmakov A and Moskovits M, 2011, Polarized Raman Scattering from a Single, Segmented SnO2 Wire, *J. Phys. Chem. C 115* pp. 17270–17277.